

**Clogging, dynamics, and reentrant fluid for active matter on periodic substrates**C. Reichhardt and C. J. O. Reichhardt *Theoretical Division and Center for Nonlinear Studies, Los Alamos National Laboratory, Los Alamos, New Mexico 87545, USA*

(Received 23 March 2021; accepted 20 May 2021; published 3 June 2021)

We examine the collective states of run-and-tumble active matter disks driven over a periodic obstacle array. When the drive is applied along a symmetry direction of the array, we find a clog-free uniform liquid state for low activity, while at higher activity, the density becomes increasingly heterogeneous and an active clogged state emerges in which the mobility is strongly reduced. For driving along nonsymmetry or incommensurate directions, there are two different clogging behaviors consisting of a drive-dependent clogged state in the low activity thermal limit and a drive-independent clogged state at high activity. These regimes are separated by a uniform flowing liquid at intermediate activity. There is a critical activity level above which the thermal clogged state does not occur, as well as an optimal activity level that maximizes the disk mobility. Thermal clogged states are dependent on the driving direction while active clogged states are not. In the low activity regime, diluting the obstacles produces a monotonic increase in the mobility; however, for large activities, the mobility is more robust against obstacle dilution. We also examine the velocity-force curves for driving along nonsymmetry directions and find that they are linear when the activity is low or intermediate but become nonlinear at high activity and show behavior similar to that found for the plastic depinning of solids. At higher drives, the active clustering is lost. For low activity, we also find a reentrant fluid phase, where the system transitions from a high mobility fluid at low drives to a clogged state at higher drives and then back into another fluid phase at very high drives. We map the regions in which the thermally clogged, partially clogged, active uniform fluid, clustered fluid, active clogged, and directionally locked states occur as a function of disk density, drift force, and activity.

DOI: [10.1103/PhysRevE.103.062603](https://doi.org/10.1103/PhysRevE.103.062603)**I. INTRODUCTION**

Active matter describes systems that have some form of self-propulsion, such as biological entities, artificial swimmers, and robots. This area is attracting increasing attention due to the experimental realization of different types of active matter, including individual or collective elements in uniform or complex environments [1,2]. One class of active matter is composed of assemblies of self-driven particles such as disks or elongated objects, in which the activity can arise from driven diffusion, run-and-tumble dynamics, chiral motion, or other forms of mobility [1,2]. In disorder-free environments, one of the most striking features of such particle-based active matter is the appearance of motility-induced phase separation [3–8], which occurs when the activity is large enough to induce a transition from a uniform fluid to a coexistence of dense or solid regions with a low-density active gas. The dense regions form even when all the pairwise interactions between the particles are repulsive.

When active-matter particles are coupled to some form of complex environment such as walls, obstacles, or pinning sites, additional behaviors can arise. These include the induced locomotion of passive objects as well as a wetting phenomenon in which active particles can align with a barrier or accumulate in corners [9–16]. If the active particles interact with a random array of obstacles, pins, or other types of quenched disorder, the clustering or flocking transition can be destroyed, and under application of a drive can be replaced

by a transition from isotropic to anisotropic cluster phases [17–22]. It is also possible for different types of trapping effects to appear [23,24], as well as transport or hopping rates that are nonmonotonic as a function of activity [25–27]. The nonmonotonicity arises because at low activity the system is easily pinned or clogged, at intermediate activity it acts like a freely flowing fluid, and at high activity it undergoes motility-induced phase separation accompanied by active clogging in which the motion is strongly reduced and occurs only intermittently or in avalanches [25,28,29].

It is also possible to place active-matter particles on a periodic array of obstacles or a periodic pinning array [30–33]. In this case, there is a well-defined average distance between the obstacles as well as clear preferred symmetry directions for motion. For nonactive particles driven over periodic arrays, strong directional locking effects occur when the direction of the drive is changed with respect to the symmetry of the underlying substrate [33–38]. The particles preferentially flow along the symmetry directions of the substrate even when the external drive is not aligned with one of those directions. As a result, a series of locking steps appear in the velocity versus driving angle curves, as has been studied for colloidal [35–37,39–42] and other driven particle systems [33,43–45] coupled to a periodic substrate. The locking can be used as a method for steering the motion of particles along certain directions or for performing particle separation in which one species locks to one symmetry direction and another species locks to another direction [46–50]. Directional

locking is the most pronounced in the single particle limit, where the existence of multiple locking directions produces a devil's staircase structure in the velocity versus angle response; however, when collective effects become important, different types of pattern formation can arise in which ordered flowing solids are stable for motion along symmetry locking directions but liquid or disordered states appear for flow along incommensurate angles [33,39–42,51].

There have been several experimental [30] and numerical studies [33,52–57] of active matter systems interacting with a periodic substrate. At large activity in the single-particle limit, the active disk motion is directionally locked even in the absence of external driving, and the prominence of this locking effect increases with increasing run times [33]. For a driven or directed active matter system, the activity can enhance the directional locking effect [30,32,33].

In this paper, we expand upon our previous studies of individual active matter disks interacting with periodic obstacle arrays [33] and consider the strongly collective regime in which clogging effects appear at both very low and very high activity. We show that different types of clogging occur depending on the direction of drive with respect to the symmetry directions of the substrate. For driving along a major symmetry direction such as  $\theta = 0^\circ$ , the system forms a uniform liquid state at low activity and the mobility monotonically decreases with increasing activity until an activity-induced cluster state emerges in which the mobility is strongly reduced. For driving along an incommensurate angle, there can be two distinct clogging phases. The first, which we call thermal clogging, is a low activity clogged state similar to the clogging studied in previous work for zero activity [58,59] and for the low activity regime of active matter on random substrates [60–62], where the active particles form a heterogeneous system-spanning cluster. The second is a high activity state called active clogging which is associated with motility-induced phase separation. There is a critical activity level above which the thermally clogged state is lost. Under a finite drive, both the thermal and active clogging depend on the active disk density. We examine the role of the driving force and find that active clogging persists down to the smallest drives since the activity itself induces the clustering effect. At higher drives, the active clogging is diminished since the drive interferes with cluster formation. In the low activity limit, we observe a reentrant fluid phase in which the system is a uniform fluid at low drives, transitions into a drive-induced clogged state, and breaks apart into a moving fluid or partially clustered state at high drives. These transitions are associated with a finite depinning threshold and negative differential mobility. For the active clogged state, there is no depinning threshold but the velocity-force curves develop nonlinearity at low drives similar to that found at plastic depinning in a nonthermal system, while at intermediate activity the velocity-force curves are linear. At high driving along incommensurate angles, for both low and high activity a directionally locked state appears in which the clustering is lost and the disks flow in strictly one-dimensional (1D) channels. In this paper, we focus on a fixed obstacle size and density. The collective effects that appear for changing obstacle size were studied in earlier work [57], where it was shown that commensuration effects arise when the spacing of the obstacle lattice matches

with the active disk size, permitting the formation of large-scale crystalline structures.

## II. SIMULATION

We consider a two-dimensional (2D) system of size  $L \times L$  with periodic boundary conditions in the  $x$  and  $y$  directions. The sample contains a square array of  $N_{\text{obs}}$  obstacles of radius  $R_{\text{obs}}$  and lattice spacing  $a$ , giving an obstacle density of  $\phi_{\text{obs}} = N_{\text{obs}}\pi R_{\text{obs}}^2/L^2$ . There are also  $N_a$  active disks with a radius of  $R_a$ . The density of the active disks is  $\phi_a = N_a\pi R_a^2/L^2$  and the total system density is  $\phi_{\text{tot}} = \phi_a + \phi_{\text{obs}}$ . After initialization, we apply a drift force  $F_D$  along either the  $x$  direction at  $\theta = 0^\circ$ , which is a symmetry direction of the obstacle array, or along  $\theta = 35^\circ$ , which is a nonsymmetry direction. In our previous work with this system in the zero activity limit at higher  $\phi_{\text{tot}}$ , we found that the disks are susceptible to clogging when  $\theta = 35^\circ$  but generally flow when  $\theta = 0^\circ$  [58].

The equation of motion for an active disk  $i$  is given by

$$\alpha_d \mathbf{v}_i = \mathbf{F}_i^{dd} + \mathbf{F}_i^m + \mathbf{F}_i^{\text{obs}} + \mathbf{F}^D. \quad (1)$$

Here  $\mathbf{v}_i = d\mathbf{r}_i/dt$  is the disk velocity,  $\mathbf{r}_i$  is the disk position, and the damping constant  $\alpha_d = 1.0$ . The active disks are modeled as run-and-tumble particles with strong harmonic repulsive interactions of the form  $\mathbf{F}_i^{dd} = \sum_{i \neq j}^{N_a} k(D_{ij} - |\mathbf{r}_{ij}|)\Theta(D_{ij} - |\mathbf{r}_{ij}|)\hat{\mathbf{r}}_{ij}$ , where  $\Theta$  is the Heaviside step function,  $D_{ij} = 2R_a$ ,  $\mathbf{r}_{ij} = \mathbf{r}_i - \mathbf{r}_j$ , and  $\hat{\mathbf{r}}_{ij} = \mathbf{r}_{ij}/|\mathbf{r}_{ij}|$ . We fix the spring constant to  $k = 100$ , which is large enough that the system behaves close to the hard disk limit over the range of forces we consider. The obstacles are also modeled as disks with the same form of harmonic repulsion but with a different radius  $R_{\text{obs}}$ , so for obstacle-disk interactions,  $D_{ij} = R_a + R_{\text{obs}}$ . In this paper, we fix  $R_{\text{obs}} = 1.0$ ,  $R_a = 0.45$ , and the obstacle lattice constant  $a = 3.0$ , giving  $\phi_{\text{obs}} = 0.349$ . We consider varied system sizes between  $L = 36$  and  $L = 72$ , but unless otherwise noted, the system size is  $L = 36$ .

The activity of the disk is produced by a motor force  $\mathbf{F}_i^m = F_M \hat{\mathbf{r}}_i^m$  where  $F_M = 1.0$  and  $\hat{\mathbf{r}}_i^m$  is a randomly chosen direction which changes instantaneously to a new completely random position on the unit circle every  $\tau_l$  time steps. All of the active disks use the same value of  $\tau_l$ , but the running of each disk is started at different randomly chosen times in the cycle so the disks do not all tumble simultaneously. Since we are working in the strongly collective regime, individual disks are likely to collide with other disks before the full time  $\tau_l$  has elapsed, producing an effective  $\tau_l$  which is shorter than the actual  $\tau_l$ . Dispersion in this effective  $\tau_l$  arises naturally and, as a result, adding dispersion to the true value of  $\tau_l$  is not likely to have a strong effect. In future work, it would be interesting to consider fat tail or bimodal distributions of  $\tau_l$ .

We quantify the activity using the run length  $l_r$ , which is the distance a single isolated active disk would move during the run time  $\tau_l$ . In general, we find that when  $l_r < 0.1a$ , the behavior is close to the thermal limit, as studied previously in the single-particle limit [33]. We note that when the motility depends on density, which is what we observe in the clustering state, it has been shown that run-and-tumble and driven diffusive active particle models can be mapped onto one another [63]. A uniform drift force  $\mathbf{F}^D = F_D \hat{\mathbf{d}}$  is applied to all the active disks, where  $\hat{\mathbf{d}}$  is along either  $\theta = 0^\circ$  or  $\theta = 35^\circ$ .

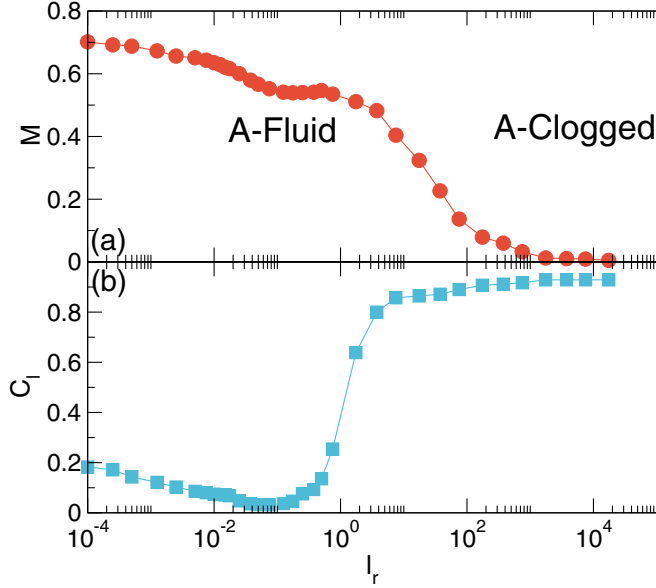


FIG. 1. (a) Mobility  $M$  versus active run length  $l_r$  for a system with a square obstacle array under a drift force  $F_D = 0.1$  applied at  $\theta = 0^\circ$  at a total density of  $\phi_{\text{tot}} = 0.622$ . (b) The corresponding fraction of disks  $C_l$  that are in the largest cluster versus  $l_r$ .  $M$  is large at low  $l_r$ , and decreases with increasing  $l_r$ , exhibiting a sharper drop that correlates with an increase in  $C_l$ . The active fluid (A-Fluid) and active clogged (A-Clogged) regimes are labeled. Error bars, which are not shown, are of order a few percent here and throughout this paper.

We characterize the transport by measuring  $\langle V_x \rangle = N_a^{-1} \sum_{i=1}^{N_a} \mathbf{v} \cdot \hat{\mathbf{x}}$  and  $\langle V_y \rangle = N_a^{-1} \sum_{i=1}^{N_a} \mathbf{v} \cdot \hat{\mathbf{y}}$ . The net velocity is given by  $\langle V \rangle = (\langle V_x \rangle^2 + \langle V_y \rangle^2)^{1/2}$ . We define the mobility of the system as  $M = \langle V \rangle / F_D$ .

### III. RESULTS

In Fig. 1(a), we plot the mobility  $M$  versus active run length  $l_r$  for a system with a fixed external drift force of  $F_D = 0.1$  applied along the  $x$  direction at  $\theta = 0^\circ$  for  $\phi_{\text{tot}} = 0.622$ . Figure 1(b) shows the corresponding fraction of disks that are in the largest cluster  $C_l$  versus  $l_r$ . To measure  $C_l$ , we identify all disks  $N_c$  which are in contact with each other in the largest cluster and divide this by the total number of active disks to obtain  $C_l = N_c / N_a$ . In Fig. 1(a),  $M \approx 0.7$  at low drives, indicating a high mobility, and gradually decreases with increasing  $l_r$ . There is a sharper decrease in  $M$  for  $l_r > 1.0$  corresponding to an increase in  $C_l$ , which indicates the onset of activity-induced clustering. For  $l_r > 1000$ ,  $M$  drops to  $M = 0.01$ , almost two orders of magnitude smaller than its value in the low activity regime.

In Fig. 2(a), we illustrate the positions of the disks and obstacles in the system from Fig. 1 for the high mobility state with  $l_r = 0.00025$ , where the disks move in 1D channels between the obstacles. There is some buckling of the channel structure, resulting in disk-obstacle collisions which reduce the mobility to  $M < 1.0$ . As  $l_r$  increases, the disk configurations become more disordered and disk-obstacle collisions become more frequent. This produces a fluctuating uniform

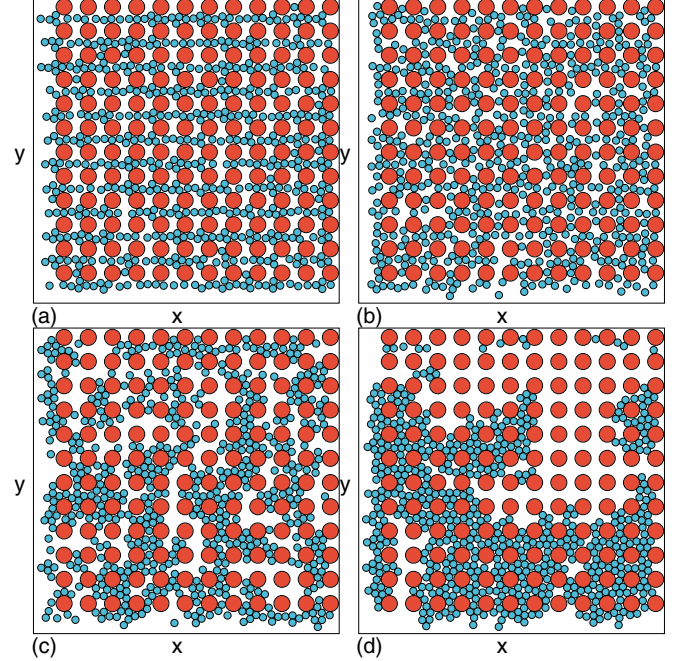


FIG. 2. Snapshots showing the active disk positions (blue) and obstacle locations (red) for the system in Fig. 1 with  $F_D = 0.1$ ,  $\phi_{\text{tot}} = 0.622$ , and  $\theta = 0^\circ$ . (a) 1D channel formation at  $l_r = 0.00025$ . (b) A uniform liquid at  $l_r = 0.175$ . (c) At  $l_r = 17.5$ , clustering begins to occur and the mobility  $M$  is reduced. (d) An active clogged state at  $l_r = 7500$ , with little motion.

liquid state in which the 1D channeling is lost and the mobility has decreased moderately, as shown in Fig. 2(b) at  $l_r = 0.175$ . At  $l_r = 17.5$  in Fig. 2(c), an active clustering effect is beginning to occur which causes a reduction in the mobility to  $M = 0.35$ , while at  $l_r = 7500$  in Fig. 2(d), the system forms an almost completely frozen cluster in what we term an active clogged state, with a mobility close to zero and only occasional small collective rearrangements. As  $l_r$  increases, the mobility decreases further, until in the infinite running time or ballistic limit,  $M = 0$ .

The results in Fig. 1 can be compared to the behavior of active matter on random substrates. In Ref. [25], the drift velocity or mobility in a random obstacle array is generally low at small  $l_r$ , reaches a maximum at intermediate  $l_r$ , and then decreases again for larger  $l_r$ . Similarly, in Ref. [28], the system is in a clogged state at low  $l_r$ , forms a liquid state for intermediate run lengths, and enters an active clogged state with nearly zero mobility at high drives. In contrast, Fig. 1 shows that there is no clogged or low mobility state at small  $l_r$  in an ordered obstacle array. Here the disks follow easy flow 1D channels between the obstacles for driving along  $\theta = 0^\circ$  at low  $\phi_{\text{tot}}$ , as illustrated in Fig. 2(a), and the mobility  $M \approx 1$  since disk-obstacle collisions are minimized. At larger  $l_r$ , an active clogged state appears regardless of whether the obstacle lattice geometry is periodic or random.

In Fig. 3, we plot  $M$  and  $C_l$  versus  $l_r$  for the same system as in Fig. 1 but with the drive applied along  $\theta = 35^\circ$ . For  $l_r < 0.01$ ,  $M \approx 0$  and  $C_l \approx 0.92$ . Here we find a nonactive or thermally clogged state of the type shown in Fig. 4(a) at  $l_r = 0.00125$ . The clogging arises from the formation of

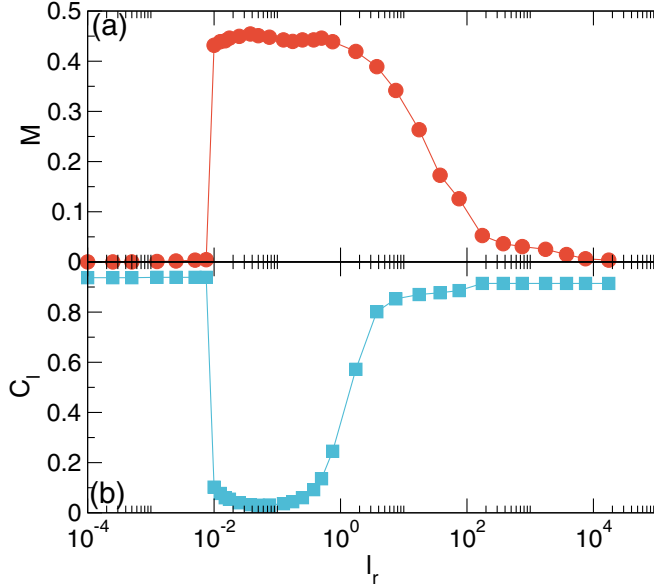


FIG. 3. (a)  $M$  versus  $l_r$  for the system in Fig. 1 with  $F_D = 0.1$  and  $\phi_{\text{tot}} = 0.622$  but where the drive is applied along  $\theta = 35^\circ$ . (b) The corresponding  $C_l$  versus  $l_r$ . Here there are two distinct clogged states: a thermally clogged state at low  $l_r$ , shown in Fig. 4(a), and an active clogged state at large  $l_r$ , shown in Fig. 4(d).

bottlenecks and arches that build up over time and block the flow. This state is similar to the  $T = 0$  clogging states studied previously for passive particles in periodic arrays [58,60,61], random arrays [62,64], and bottleneck systems [65,66], where the clogged state is associated with strongly heterogeneous particle density. We note that for smaller  $F_D$  at these small values of  $l_r$ , the activity is still large enough that the system forms a liquid rather than a clogged state, as we describe in Sec. VI.

For  $0.01 < l_r < 1.0$  in Figs. 3(a) and 3(b), a uniform liquid state appears with  $C_l < 0.2$  and a mobility of  $M \approx 0.55$ , as illustrated in Fig. 4(b) for  $l_r = 0.175$ . There is a drop in the mobility at higher  $l_r$  corresponding to the formation of an activity-induced cluster state of the type shown in Fig. 4(c) at  $l_r = 3.75$ . For  $l_r > 100$ , the system enters an actively clogged state with little motion, as shown in Fig. 4(d) at  $l_r = 7500$ .

The behavior of  $M$  versus  $l_r$  in Fig. 3 has differences from previous work on active matter driven through random arrays at low activity [28]. The transition from the passive clustered state to the active fluid state is much sharper in the periodic array. This is likely a result of the well-defined spacing between obstacles in the periodic array. The transition is better described in terms of a nucleation event, where the clustering tends to spread once one portion of the system becomes clustered. It is not clear whether this clustering or clogging transition is truly first order, and it is probably better described as an absorbing phase transition [67,68]. In general, the onset of active clustering occurs when the run length becomes larger than the distance between the obstacles. For smaller  $l_r$ , the formation of the thermally clogged state is sensitive to the direction  $\theta$  of the drive with respect to the substrate symmetry, while the active clogged state at large  $l_r$  is independent of  $\theta$ .

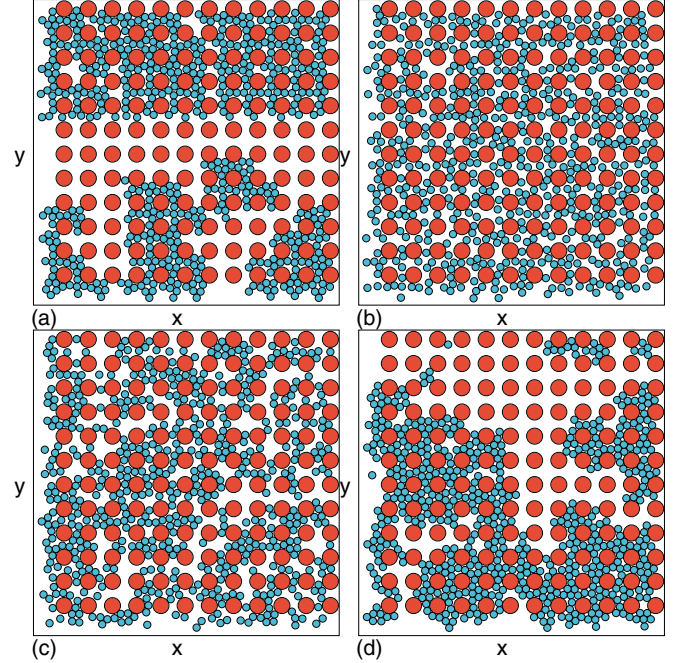


FIG. 4. Snapshots showing the active disk positions (blue) and obstacle locations (red) for the system in Fig. 3 with  $F_D = 0.1$ ,  $\phi_{\text{tot}} = 0.622$ , and  $\theta = 35^\circ$ . (a) A thermally clogged state at  $l_r = 0.00125$ . (b) A uniform liquid at  $l_r = 0.175$ . (c) At  $l_r = 3.75$ , the mobility begins to drop as clustering starts to occur. (d) An active clogged state at  $l_r = 7500$ .

Since driving along different angles can produce both thermal and active clogging, we next consider the evolution of the different phases as a function of the active disk density  $\phi_a$  for fixed  $F_D$ . In Fig. 5(a), we plot  $M$  versus  $l_r$  for the system in Fig. 3 with  $\theta = 35^\circ$  at  $\phi_{\text{tot}} = 0.6708, 0.622, 0.573, 0.5238, 0.4743, 0.4264, \text{ and } 0.3655$ , while in Fig. 5(b) we plot the corresponding  $C_l$  versus  $l_r$ . For  $\phi_{\text{tot}} > 0.5238$ , a thermally clogged state appears at small  $l_r$ , while the critical  $l_r$  at which the system transitions into the active fluid phase decreases with decreasing  $\phi_{\text{tot}}$ . When  $\phi_{\text{tot}} \leq 0.5238$ , the mobility is almost independent of  $l_r$  for small and intermediate values of  $l_r$ . For all values of  $\phi_{\text{tot}}$ , there is a transition at larger  $l_r$  to an active clustered state which is associated with a simultaneous drop in  $M$  and increase in  $C_l$ . The maximum value of  $C_l$  in the active clustered phase gradually drops with decreasing  $\phi_{\text{tot}}$  as the clusters become more spatially separated. The crossover to the active clogged state shifts to larger values of  $l_r$  as  $\phi_{\text{tot}}$  decreases.

In Fig. 6, we show a phase diagram as a function of  $l_r$  versus  $\phi_{\text{tot}}$  for the system from Figs. 3 and 5 with  $\theta = 35^\circ$ . In the active fluid, the mobility is high but no clustering occurs. For the thermally clogged state, the mobility is zero and strong clustering occurs. The thermally clogged state is present only for incommensurate driving angles such as  $\theta = 35^\circ$ , but the active clogged state is always present for sufficiently large  $l_r$  and  $\phi_{\text{tot}}$ . We use the value of the mobility to draw a distinction between the active cluster state and the active clogged state. In the active cluster state,  $C_l$  is high and  $M$  is larger than 15% of its maximum value, while in the active clogged state,  $C_l$  is also high but  $M$  is less than 15% of its maximum value.

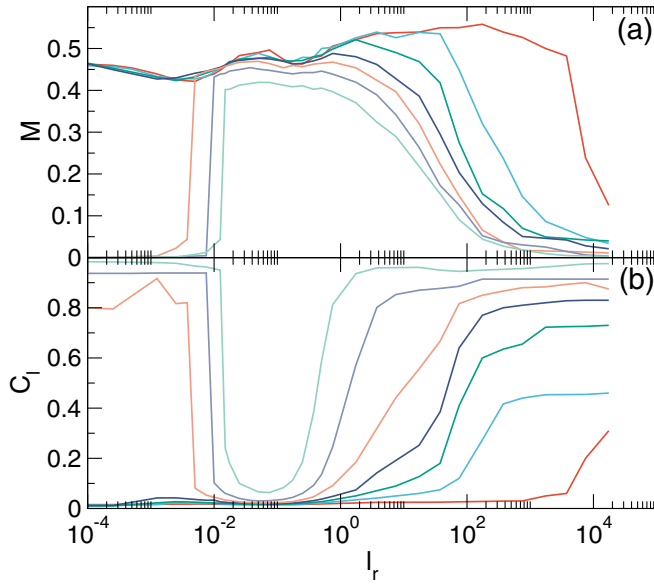


FIG. 5. (a)  $M$  versus  $l_r$  for the system in Fig. 3 with  $F_D = 0.1$  and  $\theta = 35^\circ$  for varied total density  $\phi_{\text{tot}} = 0.6708$  (light green),  $0.622$  (light purple),  $0.573$  (orange),  $0.5238$  (dark blue),  $0.4743$  (dark green),  $0.4264$  (light blue), and  $0.3655$  (dark red), from lower right to upper right. (b) The corresponding  $C_l$  versus  $l_r$ , where the curves listed above now progress from upper right to lower right.

Other definitions for the boundary of the active clogged state could be used that involve lower values of  $M$ . The transition from the active fluid to the active cluster state is best described as a crossover, as shown in Fig. 5(a). A similar phase diagram can be constructed for driving at  $\theta = 0^\circ$  (not shown). Here the thermal clogging phase is absent but it would be possible to define additional 1D and quasi-2D channeling phases at low  $l_r$  which would be distinct from the 2D uniform active fluid state. For large enough  $\phi_{\text{tot}}$  at  $\theta = 0^\circ$ , the active fluid could

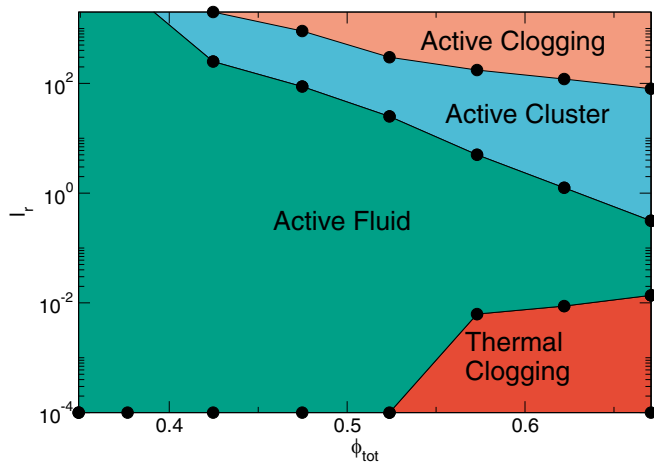


FIG. 6. Phase diagram as a function of  $l_r$  versus  $\phi_{\text{tot}}$  for the system in Figs. 3 and 5 with  $F_D = 0.1$  and  $\theta = 35^\circ$ . Green: The active fluid with uniform density, low  $C_l$ , and high  $M$ . Red: The thermally clogged phase with high  $C_l$  and  $M$  close to zero. Blue: The clustered fluid phase with high  $C_l$  and intermediate  $M$ . Orange: The active clogging phase characterized by low mobility and high  $C_l$ .

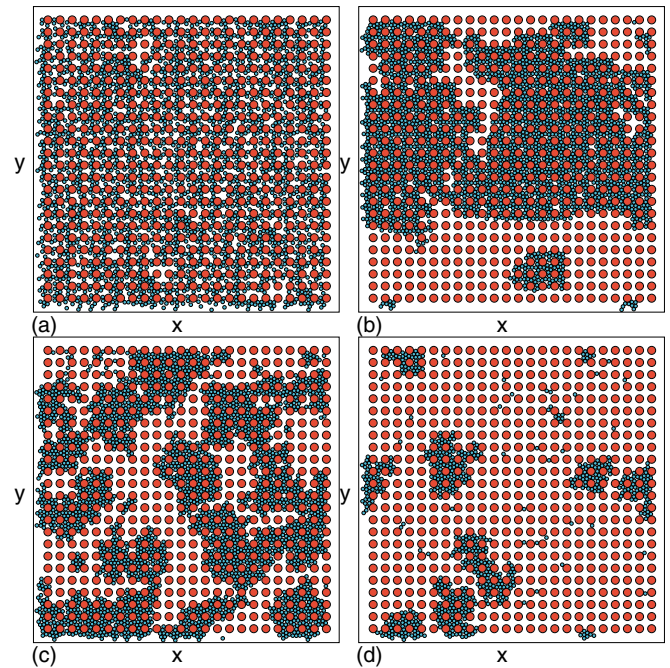


FIG. 7. Snapshots showing the active disk positions (blue) and obstacle locations (red) for driving at  $\theta = 35^\circ$  for the system in Fig. 3 with  $F_D = 0.1$  in a larger sample with  $L = 72$ . (a) A uniform state for  $\phi_{\text{tot}} = 0.622$  just after the initialization at  $l_r = 0.00125$ . (b) The same sample from (a) after the system reaches a thermally clogged state containing a large system-spanning cluster. (c) The active clogged state at  $l_r = 7500$  and  $\phi_{\text{tot}} = 0.622$  in which the clusters are not system-spanning. (d) An active clogged state at  $l_r = 7500$  and  $\phi_{\text{tot}} = 0.4265$ .

cross over into a uniform jammed state, but these extremely dense states become very computationally expensive, so we limit our study to densities at which only heterogeneous clogging occurs. Similarly, at values of  $\phi_{\text{tot}}$  larger than what we consider for the  $\theta = 35^\circ$  system in Fig. 6, a crossover could occur from the thermally clogged phase to a uniform jammed phase near  $\phi_{\text{tot}} = 0.9$  [64].

We have explored the robustness of the phases described above to changes in the system size. As shown in Fig. 7, we find similar results for a system with the same parameters as in Fig. 3 but with a larger size of  $L = 72$ . Figure 7(a) illustrates the initial state for  $\phi_{\text{tot}} = 0.622$  and  $l_r = 0.00125$  where the active disk density is still nearly uniform. In Fig. 7(b), the same sample has reached a thermally clogged state containing a large system-spanning cluster. Figure 7(c) shows the configuration in the active clogged state at  $\phi_{\text{tot}} = 0.622$  and  $l_r = 7500$ . The morphology of the clusters in the active clogged state differs from those in the thermally clogged state. The active clogged clusters are much more fragmentary and do not form a single system-spanning cluster. The thermally clogged states generally contain a cluster that is as wide as the system, while the active clogged state forms individual clusters that are each considerably smaller than the system width. This suggests that the thermally clogged state requires the total disk density to be above a 2D percolation threshold, while the active clogged state does not. In Fig. 7(d), we show an active clogged state at  $l_r = 7500$  and  $\phi_{\text{tot}} = 0.4265$ . At low  $l_r$  for

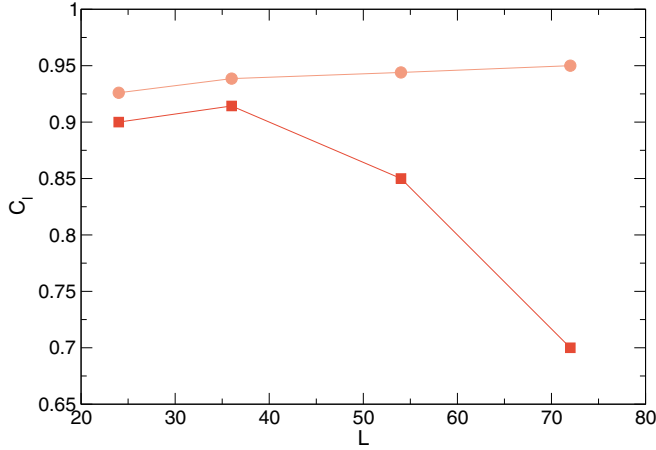


FIG. 8.  $C_l$  versus system size  $L$  for the system in Fig. 3 with  $F_D = 0.1$ ,  $\phi_{\text{tot}} = 0.622$ , and  $\theta = 35^\circ$  at  $l = 0.00125$  in the thermally clogged state (orange circles) and  $l = 7500$  in the active clogged state (red squares). The thermally clogged state is dominated by a single system-spanning cluster while the active clogged state contains multiple smaller clusters.

this same total density, the system does not form a thermally clogged state. In Fig. 8, we plot  $C_l$  versus  $L$  for the system in Fig. 3 at  $l = 0.00125$  in the thermally clogged phase and  $l = 7500$  in the active clogged phase. For the thermally clogged phase,  $C_l \lesssim 1$  independent of the system size, indicating that the system is dominated by a single system-spanning cluster as shown in Fig. 7(b). In contrast, for the active clogging phase illustrated in Fig. 7(c),  $C_l$  drops as  $L$  increases since the size of the largest cluster does not increase with system size; instead, the total number of clusters grows as  $L$  increases, so each cluster contains a smaller fraction of the total number of disks.

#### IV. DILUTED OBSTACLE ARRAYS

We next consider the effects of randomly diluting the obstacle array by removing a fraction  $D$  of the obstacles. In Figs. 9(a) and 9(b), we plot  $M$  and  $C_l$  versus the dilution factor  $D$  for the system in Fig. 3 with  $\theta = 35^\circ$ ,  $\phi_{\text{tot}} = 0.622$ , and  $F_D = 0.1$  at  $l_r = 0.00025$ , 0.005, 0.0075, 0.0175, and 0.05. For  $l_r = 0.00025$ , 0.005, and 0.0075, the thermally clogged state with  $M \approx 0$  survives at low  $D$ . The threshold for a transition to a depinned state with finite  $M$  shifts to lower values of  $D$  as  $l_r$  increases. For  $l_r = 0.00025$ , the onset of mobility occurs for  $D \approx 0.4$  and is accompanied by a small local peak in  $C_l$ . As  $D$  increases, the mobility increases monotonically, reaching  $M = 1.0$  at  $D = 1.0$  when there are no obstacles left in the system. In general,  $C_l$  decreases with increasing  $D$  and reaches  $C_l \approx 0$  for  $D = 1.0$  since the disks are no longer in contact. For  $l_r = 0.005$  and 0.0075, some clustering still persists even when  $M$  is finite due to the formation of a partially clogged state, but the clustering diminishes when  $D > 0.6$ . For  $l_r > 0.0125$ , there is no clogged state,  $M$  is finite for all values of  $D$ , and the clustering is strongly reduced.

In Figs. 9(c) and 9(d), we plot  $M$  and  $C_l$  versus  $D$  for the same system in Figs. 9(a) and 9(b) at  $l_r = 0.175$ , 17.5, 75.0, 175, and 1750. Here the average value of  $M$  decreases with

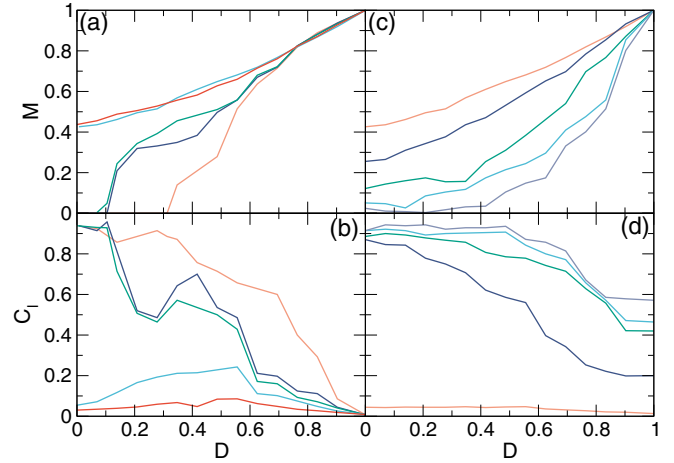


FIG. 9. (a)  $M$  and (b)  $C_l$  versus the dilution factor  $D$  for the system in Fig. 3 with  $F_D = 0.1$ ,  $\phi_{\text{tot}} = 0.622$ , and  $\theta = 35^\circ$  at  $l_r = 0.00025$  (orange), 0.005 (dark blue), 0.0075 (dark green), 0.0175 (light blue), and 0.05 (red), from lower left to upper left in  $M$  and from upper left to lower left in  $C_l$ . (c)  $M$  and (d)  $C_l$  for the same system at  $l_r = 0.175$  (orange), 17.5 (dark blue), 75.0 (dark green), 175 (light blue), and 1750 (light purple), from lower left to upper left in  $M$  and from upper left to lower left in  $C_l$ .

increasing  $l_r$ . For  $l_r = 17.5$ , the mobility remains low up to  $D = 0.2$  and then begins to increase gradually, which also correlates with the point at which the value of  $C_l$  begins to drop. For  $l_r = 75$ , the mobility increase starts near  $D = 0.4$ . For the three largest values of  $l_r$  there is a tendency for  $M$  to be flat or even decrease slightly with increasing  $D$  up to  $D = 0.4$ . This occurs because under moderate obstacle dilution, the activity-induced clusters can become more coherent or better ordered. For  $l_r = 0.175$ , there is no clustering and the mobility increases monotonically with  $D$ , while at  $l_r = 17.5$  some clustering appears for small  $D$ . In the regime of larger  $l_r$ ,  $C_l$  remains large even for  $D = 1.0$  since the clustering or motility-induced phase separation occurs for these run length values even in the absence of obstacles.

Based on the results in Fig. 9, we can identify several different phases. At low  $l_r$  and low dilution  $D$ , the system is in a thermally clogged phase with  $M \approx 0$ , while at finite dilution the system enters a partially clogged state consisting of a combination of flowing and clogged configurations, as shown in Fig. 10(a) for  $l_r = 0.005$  and  $D = 0.41$ . As a result, even though  $M$  is finite,  $C_l$  remains large. In Fig. 10(b), we illustrate the same system at  $D = 0.833$  where  $M$  is high and the clustering is strongly reduced, giving a low value of  $C_l$ . Figure 10(c) shows the uniform fluid at  $l_r = 0.175$  and  $D = 0.694$ , while in Fig. 10(d) at  $l_r = 1750$  for the same dilution, the system forms a clustered state with a reduced mobility of  $M = 0.35$ .

From the results in Fig. 10, we can construct a phase diagram as a function of  $l_r$  versus  $D$ , shown in Fig. 11. We identify a thermally clogged state in which  $M \approx 0$  and  $C_l$  is high. This is adjacent to a partially clogged state of the type shown in Fig. 10(a) containing a combination of clogged disks and mobile disks, where  $M$  is finite but  $C_l$  is high. There is a uniform fluid phase of the type illustrated in Figs. 10(b)

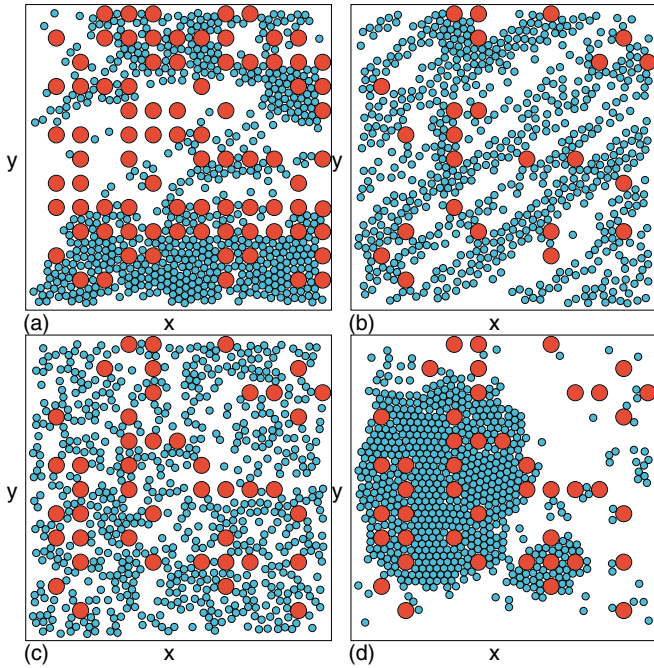


FIG. 10. Snapshots showing the active disk positions (blue) and obstacle locations (red) for the diluted system in Fig. 9 with  $F_D = 0.1$ ,  $\phi_{\text{tot}} = 0.622$ , and  $\theta = 35^\circ$ . (a) A partially clogged state at  $l_r = 0.005$  and  $D = 0.41$ . (b) Reduced clustering for  $l_r = 0.005$  and  $D = 0.833$ . (c) A uniform fluid at  $l_r = 0.175$  and  $D = 0.694$ . (d) A clustered state with reduced mobility at  $l_r = 1750$  and  $D = 0.694$ .

and 10(c) where the mobility is high and clustering is low, an active clogged phase where  $M$  is low and  $C_l$  is high, and a clustered fluid where  $M$  is high and  $C_l$  is high. The phase diagram in Fig. 11 has several similarities to the phase diagram found in experiments with colloids moving over random obstacles [61]. In particular, as the obstacle density is

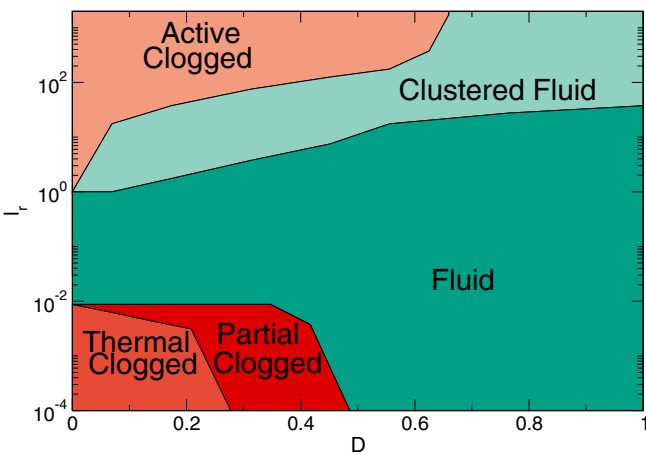


FIG. 11. Phase diagram as a function of  $l_r$  versus dilution fraction  $D$  for the system in Figs. 9 and 10 with  $F_D = 0.1$ ,  $\phi_{\text{tot}} = 0.622$ , and  $\theta = 35^\circ$ . Light red: A thermally clogged state with  $M \approx 0$  but high  $C_l$ . Dark red: A partially clogged state with intermediate  $M$  and high  $C_l$ . Dark green: A fluid phase with high  $M$  and low  $C_l$ . Light green: A clustered fluid with high  $M$  and high  $C_l$ . Orange: The active clogged state with low  $M$  and high  $C_l$ .

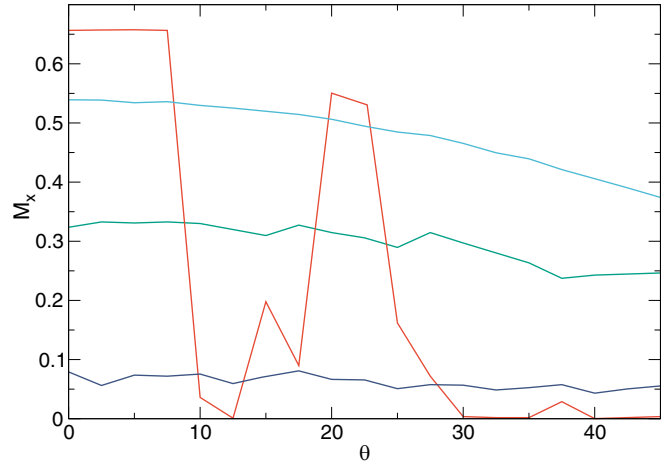


FIG. 12. The mobility in the  $x$ -direction  $M_x$  versus  $\theta$  for the system in Fig. 3 with  $F_D = 0.1$  and  $\phi_{\text{tot}} = 0.622$  at  $l_r = 0.0025$  (nonmonotonic red curve), 0.175 (light blue), 17.5 (green), and 175 (dark blue), from top to bottom for the monotonic curves.

decreased, both systems are in a clogged phase with close to zero motion when  $D$  is low, transition into partially clogged phases with intermediate velocities for intermediate  $D$ , and reach flowing phases for high  $D$ .

### V. VARIED DRIVING ANGLES

In Fig. 12, we plot the  $x$ -direction mobility  $M_x = \langle V_x \rangle / F_D$  versus driving direction  $\theta$  for the system in Fig. 3 with  $F_D = 0.1$  and  $\phi_{\text{tot}} = 0.622$  for varied  $l_r = 0.0025, 0.175, 17.5,$  and  $175$ . For  $l_r = 0.0025$ , the mobility is high for  $\theta < 10^\circ$  since the active disks are moving along quasi-1D channels similar to those shown in Fig. 2(a). For  $10^\circ \leq \theta < 20^\circ$ , a partially clogged state forms, while for  $20^\circ \leq \theta < 25^\circ$ , the active disks flow in another quasi-1D state. For  $\theta < 30^\circ$ , the thermally clogged state appears as shown earlier. The emergence of clogged states for certain driving directions and flowing states for other driving directions was also observed in  $T = 0$  passive disk studies [60]. For  $l_r = 0.175$  in Fig. 12, the system forms a uniform fluid for all values of  $\theta$  and there are no clogging phases or locking steps. For  $l_r = 17.5$ , some clustering occurs but there is still no clogging phase, and the mobility  $M_x$  is reduced at all values of  $\theta$ . At  $l_r = 175$ ,  $M_x$  is even more strongly reduced for all values of  $\theta$  but there is still no directional locking. For lower disk densities than those considered in the present paper, steps in the mobility occur at certain driving angles which correspond to symmetry directions of the obstacle array [33]. At the higher disk densities of Fig. 12, the steps disappear. These results differ from the previously studied collective behavior of  $T = 0$  nonactive systems [51] and from individual active matter particles moving on periodic obstacle arrays [33], where locking steps appeared. It may be possible that additional locking states could emerge for lower active disk densities, smaller obstacle radii, or larger  $a$ ; however, the general trend is that collective effects reduce directional locking.

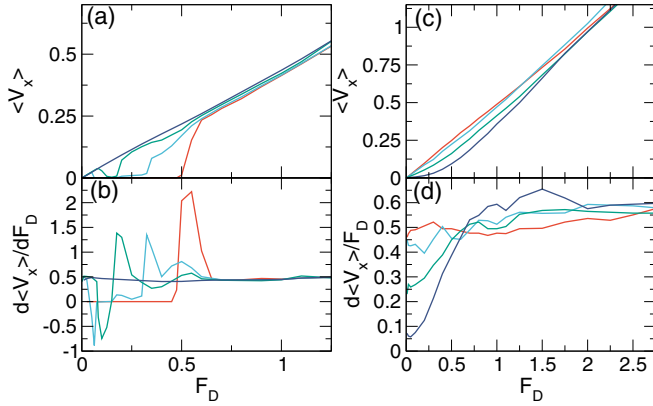


FIG. 13. (a)  $\langle V_x \rangle$  and (b)  $d\langle V_x \rangle/dF_D$  versus  $F_D$  for the system in Fig. 3 with  $\phi_{\text{tot}} = 0.67$  and  $\theta = 35^\circ$  for  $l_r = 0.00025$  (red), 0.0075 (light blue), 0.0175 (green) and 0.05 (dark blue), from bottom to top. (c)  $\langle V_x \rangle$  and (d)  $d\langle V_x \rangle/dF_D$  versus  $F_D$  for the same system at  $l_r = 0.175$  (red), 1.75 (light blue), 17.5 (green), and 175 (dark blue), from top left to bottom left.

## VI. DRIVE DEPENDENCE

We next examine the effect on the different phases of varying the magnitude of the external driving amplitude  $F_D$ . In Figs. 13(a) and 13(b), we plot  $\langle V_x \rangle$  and  $d\langle V_x \rangle/dF_D$  versus  $F_D$  for the system in Fig. 3 at  $\phi_{\text{tot}} = 0.67$  for driving along  $\theta = 35^\circ$  at  $l_r = 0.00025$ , 0.0075, 0.0175, and 0.05. At  $l_r = 0.00025$ , there is a well-defined depinning threshold near  $F_D = 0.5$  corresponding to the break up of the clogged state, which also appears as a peak in the corresponding  $d\langle V_x \rangle/dF_D$  curve. For  $l_r = 0.0075$ , an increase in  $\langle V_x \rangle$  from zero occurs near  $F_D = 0.15$ , followed by a sharper increase in  $\langle V_x \rangle$  at  $F_D = 0.3$  and a saturation in the response for  $F_D > 0.6$ . The depinning near  $F_D = 0.15$  results from the partial breakup of the clogged state into a phase where clogging and flowing disks coexist, while at the second stronger increase in  $\langle V_x \rangle$ , nearly all of the disks are flowing.

For  $l_r = 0.0075$  and 0.0175 in Figs. 13(a) and 13(b), the disks immediately begin to flow at small but nonzero  $F_D$ , but at slightly higher drives,  $\langle V_x \rangle$  drops nearly back down to zero. Here, there is a uniform fluid phase for low  $F_D$  and finite run lengths since the drive is not strong enough to cause the disks to get stuck behind obstacles. When  $F_D$  increases, however, the driving force overwhelms the activity and the disks begin to accumulate behind the obstacles, forming a clogged state in which the disks are unable to hop backward to move around the obstacles. The transition from the fluid state to the clogged state produces negative differential mobility with  $d\langle V_x \rangle/dF_D < 0$ , while in the clogged phase,  $d\langle V_x \rangle/dF_D \approx 0$ . Negative differential mobility has been observed previously for the single particle limit of passive particles driven through random obstacles, where sufficiently strong drives hold the particle trapped behind an obstacle, while under smaller drives the particle can thermally escape from behind the obstacle [69–71]. In our active system, the clogged phase at small but finite drives extends down to lower drives as  $l_r$  decreases. Even for  $l_r = 0.00025$ , there is a flowing fluid phase at drives lower than those shown in Fig. 13, but at  $l_r = 0$  the initial fluid

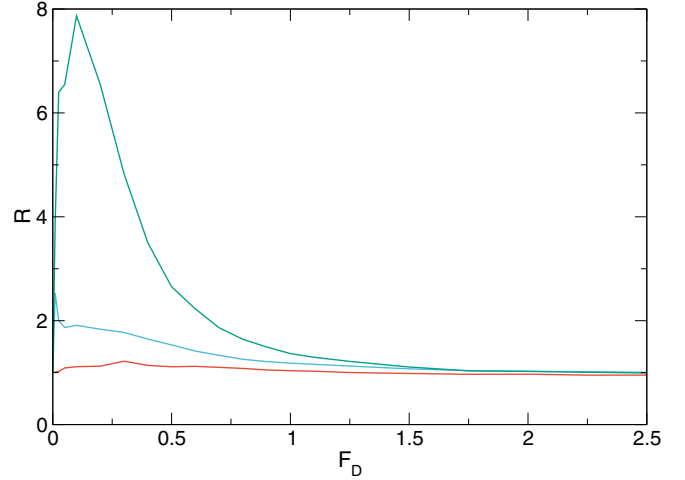


FIG. 14. The ratio  $R$  of  $\langle V_x \rangle$  divided by  $\langle V_x \rangle$  for the  $l_r = 0.175$  system from Fig. 13(c) versus  $F_D$  in samples with  $\phi_{\text{tot}} = 0.67$  and  $\theta = 35^\circ$  for  $l_r = 175$  (green), 17.5 (blue), and 1.75 (red), from top to bottom, showing that  $R$  goes to  $R = 1.0$  at large drives.

phase is lost. For  $l_r = 0.05$ , both the clogging and depinning threshold behavior are lost.

Negative differential mobility was also observed for active particles on random obstacle arrays [72] but there are some differences in the response compared to what we find for the periodic obstacle arrays. The negative differential mobility decreases when the total density of the system is increased in the random arrays, as shown in Ref. [72], whereas it increases with increasing total density in the periodic obstacle array. This is because collective clogging is responsible for the negative differential mobility in the periodic array, while individual particle trapping produces the negative differential mobility in the random array and in most other systems which display this effect.

In Figs. 13(c) and 13(d), we plot  $\langle V_x \rangle$  and  $d\langle V_x \rangle/dF_D$  versus  $F_D$  for the system from Figs. 13(a) and 13(b) at  $l_r = 0.175$ , 1.75, 17.5, and 175. For  $l_r = 0.175$ , the velocity-force curve is almost linear, which is the expected behavior for the depinning of a fluid [73]. Some deviation from linearity appears at  $l_r = 1.75$  and becomes more pronounced at  $l_r = 17.5$  and  $l_r = 175$ . The  $d\langle V_x \rangle/dF_D$  curves also show increasing nonlinearity as  $l_r$  increases, with a drop in value at low  $F_D$  followed by a linear increase and a saturation at higher  $F_D$ . There is also an overall drop in the velocity with increasing  $l_r$ . The nonlinear behavior in the velocity-force curves is similar to what is found for plastic depinning of passive particle assemblies driven over quenched disorder, such as colloids or superconducting vortices [73–76]. As the run length increases in the active disk system, the disks spend more time in a strongly clustered state and begin to act like a solid or glass coupled to random disorder. Increasing the run length is similar to decreasing the temperature in a glass. In the limit of infinite run length, we expect that there would be a true finite depinning threshold.

Figure 13(c) shows that the differences between the velocity-force curves for the different activity levels begin to disappear at higher drives. To make this more clear, in Fig. 14

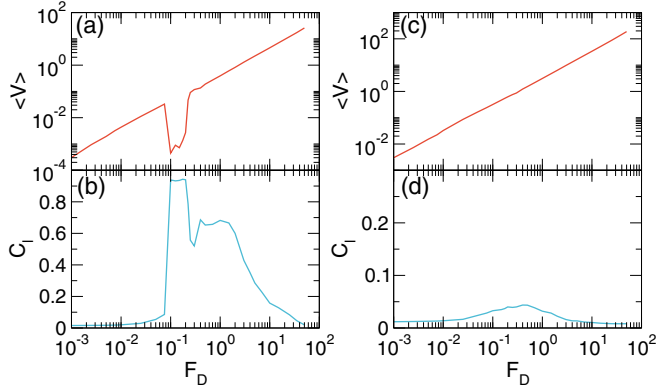


FIG. 15. (a)  $\langle V_x \rangle$  and (b)  $C_l$  versus  $F_D$  for a system with  $\phi_{\text{tot}} = 0.622$  and  $l_r = 0.0075$ . Here  $\theta = 35^\circ$ . There are four distinct phases: the low drive fluid phase illustrated in Fig. 16(a), the intermediate drive thermally clogged phase shown in Fig. 16(b), the flowing partially clustered phase appearing in Fig. 16(c), and the high drive moving liquid phase shown in Fig. 16(d). (c)  $\langle V_x \rangle$  and (d)  $C_l$  versus  $F_D$  for the same system at  $\phi_{\text{tot}} = 0.5238$ . There are only two phases: the liquid phase shown in Fig. 17(a) and the directionally locked phase flowing along  $45^\circ$ , shown in Fig. 17(b).

we plot the ratio  $R$  of  $\langle V_x \rangle$  divided by  $\langle V_x \rangle$  for the  $l_r = 0.175$  sample from Fig. 13(c) versus  $F_D$  for  $l_r = 175$ , 17.5, and 1.75. For  $l_r = 175$ , the mobility at low  $F_D$  is nearly eight times as large as in the  $l_r = 0.175$  system, but as  $F_D$  increases, the ratio of the two mobilities approaches  $R = 1.0$ . At higher drives, the collisions with obstacles become strong enough to break apart the clusters, while the driving force prevents the active disks from reorganizing into a cluster state; therefore, the system remains in a fluid state. This can also be viewed as a drive-dependent shear thinning transition in which the drive breaks up the large scale structures and thereby reduces the viscosity of the system.

#### Density dependence of the driven dynamics

As  $\phi_{\text{tot}}$  is reduced, the extent of the clogged state appearing in Figs. 13(a) and 13(b) is also reduced. To better characterize both the clogged phase and the reentrant fluid, in Figs. 15(a) and 15(b) we plot  $\langle V_x \rangle$  and  $C_l$  versus  $F_D$  for a system with  $\phi_{\text{tot}} = 0.622$  and  $l_r = 0.0075$ . In Fig. 15(a),  $\langle V_x \rangle$  increases linearly with increasing  $F_D$  up to  $F_D = 0.08$ , as expected for a fluid, and then decreases with increasing drive up to  $F_D = 0.225$ . For  $F_D < 0.08$  in Fig. 15(b),  $C_l < 0.03$  and the system forms a diffusing liquid state without any clustering. When  $0.08 < F_D < 0.225$ ,  $C_l$  jumps up to  $C_l = 0.94$  and the disks form a system-spanning thermally clogged state. The velocity does not drop completely to zero in this clogged phase since there are still occasional thermal-like jumps of the disks. For  $F_D > 0.225$ ,  $\langle V_x \rangle$  increases with increasing  $F_D$  again and there is a drop down in  $C_l$ ; however, there is still a partial clustering effect. The clustering diminishes as  $F_D$  increases, and at high drives  $C_l = 0.05$  when the system is in a uniform fluid state.

We define the different phases in Figs. 15(a) and 15(b) as a low drive uniform diffusing fluid, a thermally clogged state, a partially clustered fluid, and a high drive fluid state. The transitions between the different states appear as changes

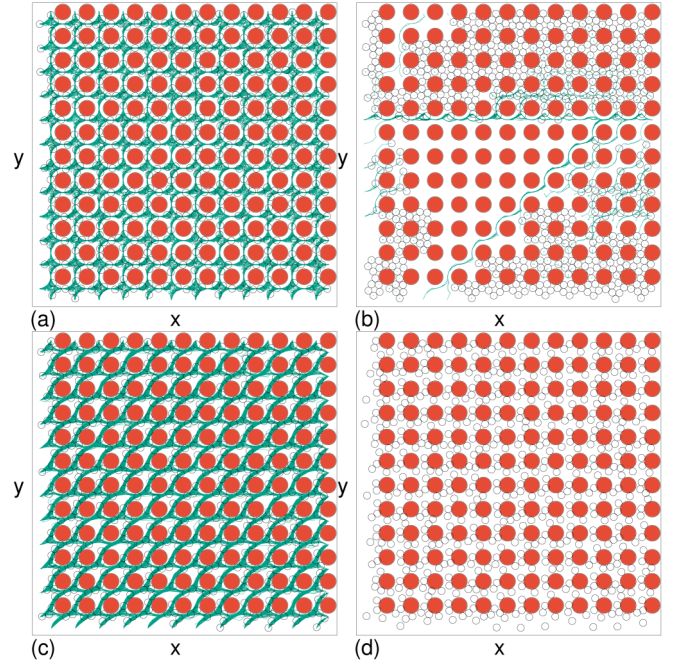


FIG. 16. The active disk positions (open circles) and trajectories (green) along with the obstacle locations (red) for the system in Figs. 15(a) and 15(b) with  $\theta = 35^\circ$ ,  $\phi_{\text{tot}} = 0.622$ , and  $l_r = 0.0075$ . (a) The moving diffusing fluid phase at  $F_D = 0.025$ . (b) The thermally clogged state at  $F_D = 0.2$ . (c) The moving partially clustered fluid at  $F_D = 0.7$ . (d) The positions of the disks without trajectories in the high drive uniform fluid at  $F_D = 15.0$ .

in  $d\langle V \rangle/dF_D$  and  $C_l$ . In studies of driven vortices, colloids, and other particle assemblies [74], different dynamical phases also appear as a function of drive; however, in most of these systems the substrate is modeled as pinning sites rather than obstacles, so the low drive fluid phase is not present. Additionally, since many of these systems have longer range particle-particle interactions, clustered or clogged states do not occur since the pairwise energy cost of strong density inhomogeneities would be too large; however, the disorder or roughening of the system is still maximized just at the depinning transition [74]. At higher drives, systems with pinning generally show a transition to an ordered state since the effectiveness of the pinning diminishes as the driving increases; however, in systems such as ours containing obstacles, the overall density becomes more uniform at higher drives but the particle positions remain disordered.

In Fig. 16(a), we plot the disk trajectories, obstacle locations, and active disk positions for the system in Fig. 15(a) at  $F_D = 0.025$  where the particles form a low drive diffusing fluid. Here there is no clustering and the trajectories are strongly disordered as the disks gradually drift along  $35^\circ$ . Figure 16(b) shows the same system at  $F_D = 0.2$  in a thermally clogged phase, where there are still some small regions of motion. At  $F_D = 0.7$  in Fig. 16(c), most of the disks are flowing in a fluid state and there is intermittent clustering. We show only the disk positions without trajectories in Fig. 16(d) for the high drive uniform fluid at  $F_D = 15.0$ , where there is no clustering but the disk positions are disordered.

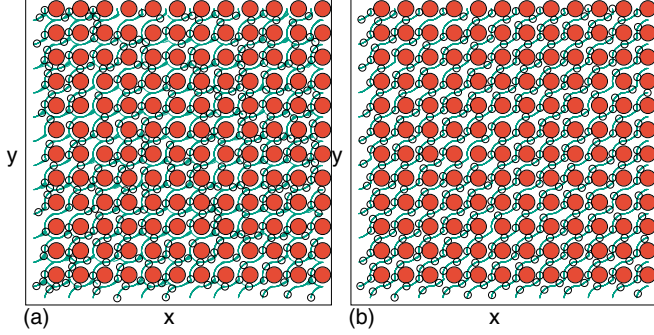


FIG. 17. The active disk positions (open circles) and trajectories (green) along with the obstacle locations (red) for the system in Figs. 15(c) and 15(d) with  $\theta = 35^\circ$ ,  $\phi_{\text{tot}} = 0.5238$ , and  $l_r = 0.0075$ . (a) At  $F_D = 0.5$ , there is a moving liquid with an average direction of motion along the driving direction of  $\theta = 35^\circ$ . (b) At  $F_D = 10.0$ , the motion occurs in nonoverlapping 1D channels locked to  $45^\circ$ .

In Figs. 15(c) and 15(d), we plot  $\langle V_x \rangle$  and  $C_l$  for the system in Figs. 15(a) and 15(b) at a lower  $\phi_{\text{tot}} = 0.5238$ . In this case, there is no clogged phase or clustering, indicating that there is a critical value of  $\phi_{\text{tot}}$  below which the clogging phase cannot occur. For low values of  $\phi_{\text{tot}}$  at lower  $F_D$ , the system forms a moving liquid phase in which the average motion is along the driving direction of  $\theta = 35^\circ$  but individual disks can diffuse over time in all directions, as shown in Fig. 17(a) for  $F_D = 0.5$ . In Fig. 18, we plot the time series of  $V_x$  and  $V_y$  for the system in Fig. 17(a). The velocities are fluctuating but the velocity components do not overlap. At higher drives, there is a transition from the diffusing fluid into a directionally locked phase with motion along  $45^\circ$  that is strictly quasi-1D

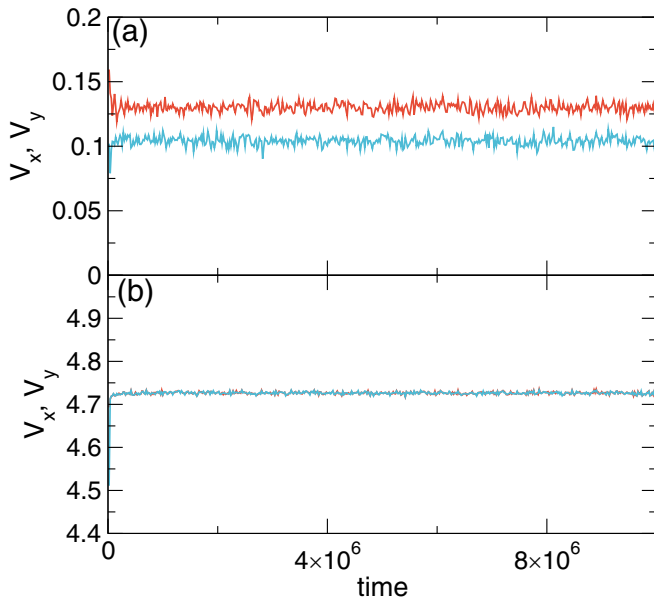


FIG. 18. The time series of the velocities  $V_x$  (top red) and  $V_y$  (bottom blue) for the system in Figs. 15(c) and 15(d) with  $\theta = 35^\circ$ ,  $\phi_{\text{tot}} = 0.5238$ , and  $l_r = 0.0075$ . (a)  $F_D = 0.5$ , where the system forms a moving fluid translating along the driving direction of  $\theta = 35^\circ$ , as shown in Fig. 17(a). (b)  $F_D = 10$ , where the motion is locked along  $45^\circ$  and occurs in 1D nonoverlapping channels.

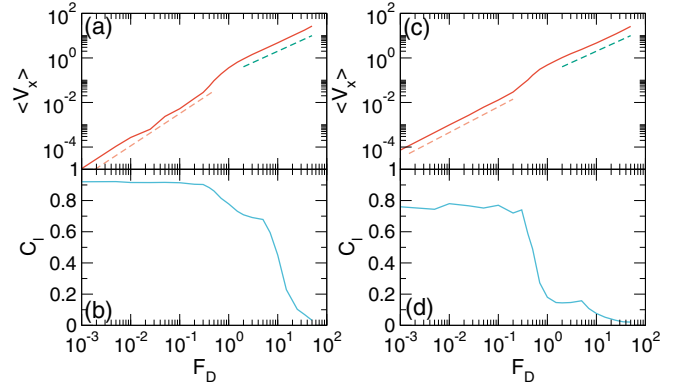


FIG. 19. (a)  $\langle V_x \rangle$  and (b)  $C_l$  versus  $F_D$  for a system with  $\theta = 35^\circ$ ,  $\phi_{\text{tot}} = 0.622$  and  $l_r = 175.0$ . The left orange dashed line is a fit to  $\langle V_x \rangle \propto F^{1.45}$ , and the right green dashed line indicates a linear dependence of  $\langle V_x \rangle$  on  $F_D$ . (c)  $\langle V_x \rangle$  and (b)  $C_l$  versus  $F_D$  for the same system at  $\phi_{\text{tot}} = 0.523$ . The left orange dashed line is a fit to  $\langle V_x \rangle \propto F^{1.15}$  and the right green dashed line is a linear fit.

without hopping between channels, as shown in Fig. 17(b) at  $F_D = 10.0$ . This transition is generally smooth as the motion gradually focuses into channels that become increasingly 1D. Here  $V_x$  and  $V_y$  have identical average values, as shown in Fig. 18(b). At even lower densities or for smaller obstacle sizes, additional directional locking phases appear.

In Figs. 19(a) and 19(b), we plot  $\langle V_x \rangle$  and  $C_l$  versus  $F_D$  for the system in Figs. 15(a) and 15(b) with  $\phi_{\text{tot}} = 0.622$  at a higher  $l_r = 175$ . Since the clustering in this regime is due to the activity,  $C_l > 0.9$  down to arbitrarily low values of  $F_D$ . This is in contrast to the drive-dependent clogging effect which appears at smaller  $l_r$ . Near  $F_D = 0.5$ , there is a change in the velocity-force curve corresponding to a drop in  $C_l$ , while a second small cusp in  $C_l$  is visible near  $F_D = 7.0$ . For  $F_D < 0.5$ , the system is in the active clogged state and the velocity-force curve is nonlinear, as indicated by the orange dashed line, which shows a power-law fit to  $\langle V_x \rangle \propto F_D^{1.45}$ . Above the cusp in  $\langle V_x \rangle$ , the green dashed line indicates that the behavior is linear with  $\langle V_x \rangle \propto F_D$ . For passive 2D systems with quenched disorder at  $T = 0$ , plastic flow regimes are associated with a velocity-force signature of  $V \propto F^\alpha$  with  $1.33 < \alpha < 2.0$ , where  $\alpha \approx 1.5$  is often observed [73,74,76]. The fits shown in Fig. 19 with  $\alpha > 1.33$  resemble the signatures found in the plastic depinning transition of a glasslike state [76,77], while systems with long-range interactions between particles often give exponents close to  $\alpha = 2$  [78]. In contrast, when elastic depinning occurs, as for a rigid solid,  $\alpha \sim 1/3$  [79]. This suggests that the active clogged regime behaves like a plastically distorting solid moving over quenched disorder. At higher drives, the self-clustering starts to break down and the velocity response becomes linear, as expected for a strongly driven fluid in quenched disorder [71,74].

In Figs. 19(c) and 19(d), we plot  $\langle V_x \rangle$  and  $C_l$  versus  $F_D$  for the system from Figs. 19(a) and 19(b) at a lower  $\phi_{\text{tot}} = 0.523$ . We find a similar behavior in which the system starts out in a clustered state at low drives and transitions to a moving fluid at higher drives. There is a cusp in  $\langle V_x \rangle$  near  $F_D = 1.0$  which corresponds to a drop in  $C_l$ . Below the cusp,  $\langle V_x \rangle \propto F^{1.15}$ , while above the cusp,  $\langle V_x \rangle \propto F^{1.0}$ . This suggests that although

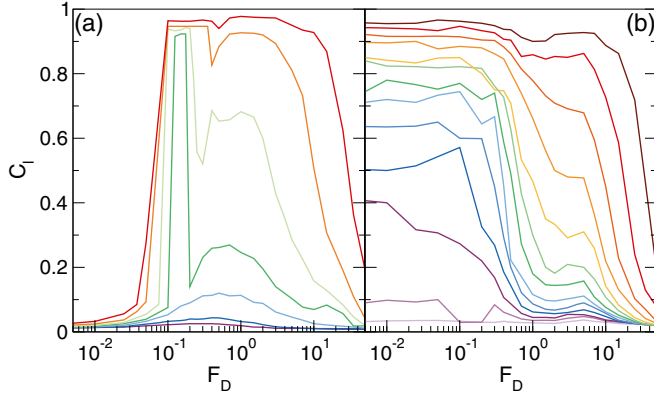


FIG. 20. (a)  $C_l$  versus  $F_D$  for a system with  $\theta = 35^\circ$  at a fixed  $l_r = 0.0075$  for varied  $\phi_{\text{tot}} = 0.671$  (red), 0.6465 (orange), 0.622 (light green), 0.59744 (dark green), 0.5729 (light blue), 0.5238 (dark blue), and 0.475 (purple), from top to bottom. (b)  $C_l$  versus  $F_D$  for the same system at  $l_r = 175$  at  $\phi_{\text{tot}} = 0.671$  (brown), 0.6465 (red), 0.622 (dark orange), 0.59744 (medium orange), 0.5729 (light orange), 0.548 (light green), 0.5238 (dark green), 0.5 (light blue), 0.475 (medium blue), 0.45 (dark blue), 0.4256 (dark purple), 0.401 (medium purple), and 0.3765 (light purple), from top to bottom.

clustering is occurring at the lower drives, the cluster sizes are smaller compared to the  $l_r = 175$  case. As a result, the system behaves more like a fluid than like a plastically moving solid. There is also a small cusp in  $C_l$  near  $F_D = 5.0$  which corresponds to the transition from a moving fluid to locked flow along  $45^\circ$ .

In Fig. 20(a), we plot  $C_l$  versus  $F_D$  for a system with fixed  $l_r = 0.0075$  at varied  $\phi_{\text{tot}} = 0.671, 0.6465, 0.622, 0.59744, 0.5729, 0.5238,$  and  $0.475$ . The four phases are clearly visible. In the low drive fluid phase,  $C_l < 0.1$ . The clogged phase corresponds to the peak in  $C_l$ , while the partially clustered liquid with  $C_l > 0.5$  appears above the clogging peak. At high drives, there is a liquid with  $C_l < 0.5$ . The width of the clogged phase decreases with decreasing  $\phi_{\text{tot}}$ . For  $\phi_{\text{tot}} = 0.59744$ , the system passes directly from the clogged state to the liquid phase, while for  $\phi_{\text{tot}} < 0.59744$ , the system is always in a fluid state at lower drives and reaches a directionally locked phase with motion along  $45^\circ$  at higher drives.

In Fig. 21(a), we plot a phase diagram as a function of  $\phi_{\text{tot}}$  versus  $F_D$  for the system in Fig. 20(a) with  $l_r = 0.0075$ . The transitions between the phases are obtained based on the behavior of  $C_l$ , the velocities, and the trajectories. At low  $F_D$  and low  $\phi_{\text{tot}}$  we find a fluid phase, while at high  $F_D$  a 1D locked phase with motion along  $45^\circ$  emerges. For  $\phi_{\text{tot}} \geq 0.59744$ , both clogged and reentrant fluid phases can occur. The boundaries of the clustered fluid phase shift at different rates to higher  $F_D$  with increasing  $\phi_{\text{tot}}$ , causing the clustered fluid to increase in extent for larger  $\phi_{\text{tot}}$ . The transition from the fluid to the symmetry-locked flow along  $45^\circ$  shifts to lower drives with decreasing  $\phi_{\text{tot}}$ .

In Fig. 20(b), we plot  $C_l$  versus  $F_D$  for the system in Fig. 20(a) at  $l_r = 175$  for  $\phi = 0.671, 0.6465, 0.622, 0.59744, 0.5729, 0.548, 0.5238, 0.5, 0.475, 0.45, 0.4256, 0.401,$  and  $0.3765$ . We find clustering with  $C_l > 0.5$  for lower drives when  $\phi_{\text{tot}} > 0.4256$ . The transition from the cluster phase to a

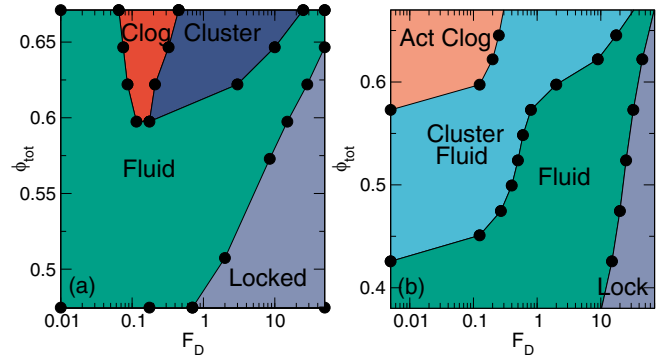


FIG. 21. (a) Phase diagram as a function of  $\phi_{\text{tot}}$  versus  $F_D$  for the system in Fig. 20(a) with  $\theta = 35^\circ$  at  $l_r = 0.0075$ , showing the reentrant fluid phase (green), the thermally clogged phase (red), the partially clustered moving phase (blue) and the directionally locked phase (light purple). (b) Phase diagram as a function of  $\phi_{\text{tot}}$  versus  $F_D$  for the system in Fig. 20(b) with  $l_r = 175$ , showing the active clogged phase (orange), the clustered fluid (blue), the fluid phase (green), and the directionally locked phase (light purple).

moving state shifts to lower  $F_D$  as  $\phi_{\text{tot}}$  is reduced. Additionally, for higher drives, the system enters the 1D locking phase with motion along  $45^\circ$ . In general, as  $l_r$  increases, a higher driving force is needed to reach the locked state. In Fig. 21(b), we plot a phase diagram as a function of  $\phi_{\text{tot}}$  versus  $F_D$  for the system in Fig. 20(b) highlighting the four phases. The active clogged phase is defined to occur when  $M$  is below 15% of its maximum value and  $C_l$  is large. The clustered phase appears when  $C_l > 0.5$  and  $M$  is greater than 15% of its maximum value. In the fluid phase, the mobility is high and there is no clustering, while in the locked phase, there is 1D motion along  $45^\circ$ . Compared to the system with a lower value of  $l_r$  in Fig. 21(a), when  $l_r$  is higher, the clogging and cluster phases extend to lower  $\phi_{\text{tot}}$  and larger  $F_D$ .

In Fig. 22, we plot a phase diagram as a function of  $F_D$  versus  $l_r$  for the system in Fig. 21 at fixed  $\phi_{\text{tot}} = 0.622$ , showing the relationships between the thermally clogged phase, the reentrant fluid phase, and the active clogged phase. At finite but low  $F_D$  and small  $l_r$ , the thermally clogged phase appears and its onset shifts to higher  $F_D$  with increasing  $l_r$  until it is completely lost for  $l_r > 0.025$ . The clogged phase extends all the way down to  $F_D = 0$  only when  $l_r$  reaches zero. Under increasing  $F_D$ , there is a crossover from the zero mobility thermally clogged phase to the low-mobility partially clogged phase composed of coexisting clogged and moving disks. Another transition occurs at higher drives to a uniform fluid with high  $M$  and low  $C_l$ . When  $l_r > 1.0$ , an active clogged state and active clustered fluid appear for low drives. Unlike the thermally clogged state, the active clogged state can persist down to  $F_D = 0$  since the clustering is produced by the activity instead of by the driving. For all values of  $l_r$ , once  $F_D$  becomes sufficiently large, the system enters a locked phase of 1D flow along  $45^\circ$ . For driving along  $\theta = 0^\circ$ , the thermally clogged and partially clogged phases at small  $l_r$  are absent, while the locked flow along  $45^\circ$  is replaced by locked flow along  $0^\circ$ . For other driving angles  $\theta$ , the widths of the thermally clogged, partially clogged, and fluid phases vary, but the active clogged phases persist.

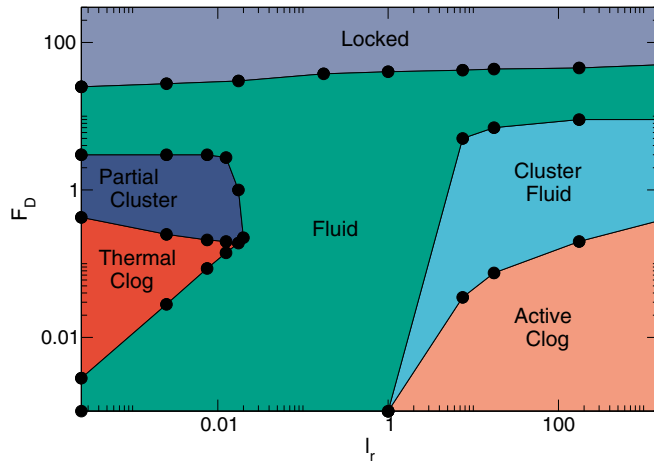


FIG. 22. The phase diagram as a function of  $F_D$  versus  $l_r$  for the system in Fig. 20 with  $\theta = 35^\circ$  for a fixed  $\phi_{\text{tot}} = 0.622$ , showing the thermally clogged phase (red), the fluid phase (green), a partially clustered fluid phase (dark blue), an active clogged phase (orange), an active clustered fluid phase (light blue), and the directionally locked 1D flow along  $45^\circ$  (light purple).

## VII. DISCUSSION

Throughout this paper we considered a square obstacle lattice, which is a convenient choice since the two easy-flow directions are orthogonal to one another. If a triangular lattice of obstacles were used instead, the general results would be the same, but for short running lengths, the angles at which reduced clogging occurs or where clogging is enhanced will differ. For the square lattice, motion along  $0^\circ$  and  $90^\circ$  is the least susceptible to clogging, while for the triangular lattice, such motion would occur along  $0^\circ$  and  $60^\circ$ . In the long running length limit, the effect of the obstacle lattice geometry is lost so there would not be any difference between the two obstacle lattices in the active clogging regime. At very high drives, the motion can lock to 1D channels, which would be along  $60^\circ$ ,  $30^\circ$ , and  $0^\circ$  for the triangular lattice instead of along  $90^\circ$ ,  $45^\circ$ , and  $0^\circ$  as in the square lattice. Behavior of this type has been observed previously for the motion of particles over a triangular lattice [41,80–82].

We considered only monotonically increasing driving forces. In future studies, it would be interesting to consider what happens if the driving force were instead cycled or if the direction of driving was gradually rotated. Such a study could be used to construct parametric plots of the cluster size  $C_l$  and the mobility  $M$ . We also did only a limited study of the velocity time series, but in future work a fuller exploration of the velocity noise, power spectra, fluctuations, and distributions could be performed for each of the different states, similar to studies performed in other systems [83–86]. This would provide more detailed information about the manner in which intermittent motion emerges near the clogging transition. The evolution of the cluster size over time would also be an interesting quantity to measure, as would the differences in the distributions of cluster sizes between the active and passive clogging regimes.

## VIII. SUMMARY

We have numerically examined run-and-tumble active disks moving over a periodic obstacle array in the collective limit. For driving along the  $x$  axis, we find that the system forms an active clustered state and an active clogged state at large run lengths. The onset of clustering is associated with a drop in the mobility. For driving at an incommensurate angle, we find two distinct clogging phases: a heterogeneous thermally clogged state at low activity, and an active clogged state at large activity. The two phases are separated by a uniform fluid state, and there is an active clustered state between the active clogged state and the fluid state. The thermally clogged state is strongly sensitive to whether the driving is along a symmetry direction of the substrate or whether it is along an incommensurate angle, while the active clogged state is independent of the driving direction. The thermally clogged state is always system spanning and involves the formation of a single large cluster, while the active clogged state contains multiple smaller clusters which are scattered throughout the sample. When the obstacle lattice is diluted via the random removal of a fraction of the obstacles, there is a critical dilution fraction above which the thermally clogged state is lost; however, the active clogged state is much more robust against dilution. We observe a reentrant fluid phase as a function of driving force in the low activity regime. For finite activity, the system can always flow when the drive is low enough, but as the drive increases, a drive dependent clogged state appears that can depin for sufficiently high driving. This drive dependent clogged state is associated with negative differential mobility in the velocity-force curves. Above depinning, there is a partially clogged state consisting of coexisting clogged and moving regions, while a moving uniform fluid appears at higher drives. In the active clogging regime, the velocity-force curves are nonlinear and can be fit to  $V \propto F^\alpha$  with  $\alpha > 1.33$ , similar to the behavior observed in plastically flowing passive solids moving over quenched disorder. At higher drives, the active clusters break apart and a moving fluid appears. We map out phase diagrams to identify the locations of the reentrant fluid state, thermal clogging, a partially clustered phase, active clogging, and an active clustered state. We also find that at high drives, the system undergoes directionally locked flow through 1D channels aligned with a symmetry direction of the obstacle lattice. Our results demonstrate how a driven active system can transition from thermal clogging behavior to active clogging behavior as a function of increasing activity.

## ACKNOWLEDGMENTS

We gratefully acknowledge the support of the US Department of Energy through the LANL/LDRD program for this work. This work was supported by the US Department of Energy through the Los Alamos National Laboratory. Los Alamos National Laboratory is operated by Triad National Security, LLC, for the National Nuclear Security Administration of the US Department of Energy (Contract No. 892333218NCA000001).

- [1] M. C. Marchetti, J. F. Joanny, S. Ramaswamy, T. B. Liverpool, J. Prost, M. Rao, and R. A. Simha, Hydrodynamics of soft active matter, *Rev. Mod. Phys.* **85**, 1143 (2013).
- [2] C. Bechinger, R. Di Leonardo, H. Löwen, C. Reichhardt, G. Volpe, and G. Volpe, Active particles in complex and crowded environments, *Rev. Mod. Phys.* **88**, 045006 (2016).
- [3] Y. Fily and M. C. Marchetti, Athermal Phase Separation of Self-Propelled Particles with no Alignment, *Phys. Rev. Lett.* **108**, 235702 (2012).
- [4] G. S. Redner, M. F. Hagan, and A. Baskaran, Structure and Dynamics of a Phase-Separating Active Colloidal Fluid, *Phys. Rev. Lett.* **110**, 055701 (2013).
- [5] J. Palacci, S. Sacanna, A. P. Steinberg, D. J. Pine, and P. M. Chaikin, Living crystals of light-activated colloidal surfers, *Science* **339**, 936 (2013).
- [6] I. Buttinoni, J. Bialké, F. Kümmel, H. Löwen, C. Bechinger, and T. Speck, Dynamical Clustering and Phase Separation in Suspensions of Self-Propelled Colloidal Particles, *Phys. Rev. Lett.* **110**, 238301 (2013).
- [7] M. E. Cates and J. Tailleur, Motility-induced phase separation, *Annu. Rev. Condens. Matter Phys.* **6**, 219 (2015).
- [8] C. Reichhardt and C. J. O. Reichhardt, Absorbing phase transitions and dynamic freezing in running active matter systems, *Soft Matter* **10**, 7502 (2014).
- [9] X. Yang, M. L. Manning, and M. C. Marchetti, Aggregation and segregation of confined active particles, *Soft Matter* **10**, 6477 (2014).
- [10] S. A. Mallory, C. Valeriani, and A. Cacciuto, Curvature-induced activation of a passive tracer in an active bath, *Phys. Rev. E* **90**, 032309 (2014).
- [11] S. C. Takatori, W. Yan, and J. F. Brady, Swim Pressure: Stress Generation in Active Matter, *Phys. Rev. Lett.* **113**, 028103 (2014).
- [12] D. Ray, C. Reichhardt, and C. J. Olson Reichhardt, Casimir effect in active matter systems, *Phys. Rev. E* **90**, 013019 (2014).
- [13] R. Ni, M. A. Cohen Stuart, and P. G. Bolhuis, Tunable Long Range Forces Mediated by Self-Propelled Colloidal Hard Spheres, *Phys. Rev. Lett.* **114**, 018302 (2015).
- [14] C. J. O. Reichhardt and C. Reichhardt, Ratchet effects in active matter systems, *Annu. Rev. Condens. Matter Phys.* **8**, 51 (2017).
- [15] A. P. Solon, Y. Fily, A. Baskaran, M. E. Cates, Y. Kafri, M. Kardar, and J. Tailleur, Pressure is not a state function for generic active fluids, *Nat. Phys.* **11**, 673 (2015).
- [16] T. Speck, Collective forces in scalar active matter, *Soft Matter* **16**, 2652 (2020).
- [17] O. Chepizhko, E. G. Altmann, and F. Peruani, Optimal Noise Maximizes Collective Motion in Heterogeneous Media, *Phys. Rev. Lett.* **110**, 238101 (2013).
- [18] A. Morin, N. Desreumaux, J.-B. Caussin, and D. Bartolo, Distortion and destruction of colloidal flocks in disordered environments, *Nat. Phys.* **13**, 63 (2017).
- [19] C. Sándor, A. Libál, C. Reichhardt, and C. J. O. Reichhardt, Dewetting and spreading transitions for active matter on random pinning substrates, *J. Chem. Phys.* **146**, 204903 (2017).
- [20] D. Yllanes, M. Leoni, and M. C. Marchetti, How many dissenters does it take to disorder a flock? *New J. Phys.* **19**, 103026 (2017).
- [21] C. Sándor, A. Libál, C. Reichhardt, and C. J. O. Reichhardt, Dynamic phases of active matter systems with quenched disorder, *Phys. Rev. E* **95**, 032606 (2017).
- [22] A. Chardac, S. Shankar, M. C. Marchetti, and D. Bartolo, Emergence of dynamic vortex glasses in disordered polar active fluids, *PNAS* **118**, e2018218118 (2021).
- [23] T. Bhattacharjee and S. S. Dutta, Bacterial hopping and trapping in porous media, *Nat. Commun.* **10**, 2075 (2019).
- [24] S. Shi, H. Li, G. Feng, W. Tian, and K. Chen, Transport of self-propelled particles across a porous medium: Trapping, clogging, and the Matthew effect, *Phys. Chem. Chem. Phys.* **22**, 14052 (2020).
- [25] C. Reichhardt and C. J. O. Reichhardt, Active matter transport and jamming on disordered landscapes, *Phys. Rev. E* **90**, 012701 (2014).
- [26] A. Morin, D. Lopes Cardozo, V. Chikkadi, and D. Bartolo, Diffusion, subdiffusion, and localization of active colloids in random post lattices, *Phys. Rev. E* **96**, 042611 (2017).
- [27] T. Bertrand, Y. Zhao, O. Bénichou, J. Tailleur, and R. Voituriez, Optimized Diffusion of Run-and-Tumble Particles in Crowded Environments, *Phys. Rev. Lett.* **120**, 198103 (2018).
- [28] C. Reichhardt and C. J. O. Reichhardt, Clogging and depinning of ballistic active matter systems in disordered media, *Phys. Rev. E* **97**, 052613 (2018).
- [29] C. J. O. Reichhardt and C. Reichhardt, Avalanche dynamics for active matter in heterogeneous media, *New J. Phys.* **20**, 025002 (2018).
- [30] G. Volpe, I. Buttinoni, D. Vogt, H.-J. Kümmerer, and C. Bechinger, Microswimmers in patterned environments, *Soft Matter* **7**, 8810 (2011).
- [31] C. Lozano, B. ten Hagen, H. Löwen, and C. Bechinger, Phototaxis of synthetic microswimmers in optical landscapes, *Nat. Commun.* **7**, 12828 (2016).
- [32] M. Brun-Cosme-Bruny, A. Förtsch, W. Zimmermann, E. Bertin, P. Peyla, and S. Rafaï, Deflection of phototactic microswimmers through obstacle arrays, *Phys. Rev. Fluids* **5**, 093302 (2020).
- [33] C. Reichhardt and C. J. O. Reichhardt, Directional locking effects for active matter particles coupled to a periodic substrate, *Phys. Rev. E* **102**, 042616 (2020).
- [34] C. Reichhardt and F. Nori, Phase Locking, Devil's Staircases, Farey Trees, and Arnold Tongues in Driven Vortex Lattices with Periodic Pinning, *Phys. Rev. Lett.* **82**, 414 (1999).
- [35] P. T. Korda, M. B. Taylor, and D. G. Grier, Kinetically Locked-in Colloidal Transport in an Array of Optical Tweezers, *Phys. Rev. Lett.* **89**, 128301 (2002).
- [36] A. Gopinathan and D. G. Grier, Statistically locked-in Transport through Periodic Potential Landscapes, *Phys. Rev. Lett.* **92**, 130602 (2004).
- [37] M. Balvin, E. Sohn, T. Iracki, G. Drazer, and J. Frechette, Directional Locking and the Role of Irreversible Interactions in Deterministic Hydrodynamics Separations in Microfluidic Devices, *Phys. Rev. Lett.* **103**, 078301 (2009).
- [38] J. Koplik and G. Drazer, Nanoscale simulations of directional locking, *Phys. Fluids* **22**, 052005 (2010).
- [39] C. Reichhardt and C. J. O. Reichhardt, Dynamical Ordering and Directional Locking for Particles Moving over Quasicrystalline Substrates, *Phys. Rev. Lett.* **106**, 060603 (2011).
- [40] T. Bohlein and C. Bechinger, Experimental Observation of Directional Locking and Dynamical Ordering of Colloidal

- Monolayers Driven Across Quasiperiodic Substrates, *Phys. Rev. Lett.* **109**, 058301 (2012).
- [41] R. L. Stoop, A. V. Straube, T. H. Johansen, and P. Tierno, Collective Directional Locking of Colloidal Monolayers on a Periodic Substrate, *Phys. Rev. Lett.* **124**, 058002 (2020).
- [42] X. Cao, E. Panizon, A. Vanossi, N. Manini, and C. Bechinger, Orientational and directional locking of colloidal clusters driven across periodic surfaces, *Nat. Phys.* **15**, 776 (2019).
- [43] A. V. Silhanek, L. Van Look, S. Raedts, R. Jonckheere, and V. V. Moshchalkov, Guided vortex motion in superconductors with a square antidot array, *Phys. Rev. B* **68**, 214504 (2003).
- [44] N. P. Vizarim, C. Reichhardt, C. J. O. Reichhardt, and P. A. Venegas, Skyrmion dynamics and topological sorting on periodic obstacle arrays, *New J. Phys.* **22**, 053025 (2020).
- [45] J. Feilhauer, S. Saha, J. Tobik, M. Zelent, L. J. Heyderman, and M. Mruczkiewicz, Controlled motion of skyrmions in a magnetic antidot lattice, *Phys. Rev. B* **102**, 184425 (2020).
- [46] M. P. MacDonald, G. C. Spalding, and K. Dholakia, Microfluidic sorting in an optical lattice, *Nature (London)* **426**, 421 (2003).
- [47] L. R. Huang, E. C. Cox, R. H. Austin, and J. C. Sturm, Continuous particle separation through deterministic lateral displacement, *Science* **304**, 987 (2004).
- [48] S. R. Risbud and G. Drazer, Directional locking in deterministic lateral-displacement microfluidic separation systems, *Phys. Rev. E* **90**, 012302 (2014).
- [49] Y. Roichman, V. Wong, and D. G. Grier, Colloidal transport through optical tweezer arrays, *Phys. Rev. E* **75**, 011407 (2007).
- [50] B. R. Long, M. Heller, J. P. Beech, H. Linke, H. Bruus, and J. O. Tegenfeldt, Multidirectional sorting modes in deterministic lateral displacement devices, *Phys. Rev. E* **78**, 046304 (2008).
- [51] C. Reichhardt and C. J. O. Reichhardt, Collective effects and pattern formation for directional locking of disks moving through obstacle arrays, *Phys. Rev. E* **102**, 022608 (2020).
- [52] M. Zeitz, K. Wolff, and H. Stark, Active Brownian particles moving in a random Lorentz gas, *Eur. Phys. J. E* **40**, 23 (2017).
- [53] S. Pattanayak, R. Das, M. Kumar, and S. Mishra, Enhanced dynamics of active Brownian particles in periodic obstacle arrays and corrugated channels, *Eur. Phys. J. E* **42**, 62 (2019).
- [54] R. Alonso-Matilla, B. Chakrabarti, and D. Saintillan, Transport and dispersion of active particles in periodic porous media, *Phys. Rev. Fluids* **4**, 043101 (2019).
- [55] K. Schakenraad, L. Ravazzano, N. Sarkar, J. A. J. Wondergem, R. M. H. Merks, and L. Giomi, Topotaxis of active Brownian particles, *Phys. Rev. E* **101**, 032602 (2020).
- [56] H. E. Ribeiro, W. P. Ferreira, and Fabrício Q. Potiguar, Trapping and sorting of active matter in a periodic background potential, *Phys. Rev. E* **101**, 032126 (2020).
- [57] C. Reichhardt and C. J. O. Reichhardt, Active matter commensuration and frustration effects on periodic substrates, *Phys. Rev. E* **103**, 022602 (2021).
- [58] H. T. Nguyen, C. Reichhardt, and C. J. O. Reichhardt, Clogging and jamming transitions in periodic obstacle arrays, *Phys. Rev. E* **95**, 030902(R) (2017).
- [59] H. Peter, A. Libál, C. Reichhardt, and C. J. O. Reichhardt, Crossover from jamming to clogging behaviours in heterogeneous environments, *Sci. Rep.* **8**, 10252 (2018).
- [60] C. Reichhardt and C. J. O. Reichhardt, Directional clogging and phase separation for disk flow through periodic and diluted obstacle arrays, *Soft Matter* **17**, 1548 (2021).
- [61] R. L. Stoop and P. Tierno, Clogging and jamming of colloidal monolayers driven across disordered landscapes, *Commun. Phys.* **1**, 68 (2018).
- [62] S. G. Leyva, R. L. Stoop, P. Tierno, and I. Pagonabarraga, Dynamics and clogging of colloidal monolayers magnetically driven through a heterogeneous landscape, *Soft Matter* **16**, 6985 (2020).
- [63] M. E. Cates and J. Tailleur, When are active Brownian particles and run-and-tumble particles equivalent? Consequences for motility-induced phase separation, *EPL* **101**, 20010 (2013).
- [64] C. Reichhardt and C. J. O. Reichhardt, Aspects of jamming in two-dimensional athermal frictionless systems, *Soft Matter* **10**, 2932 (2014).
- [65] I. Zuriguel, D. R. Parisi, R. C. Hidalgo, C. Lozano, A. Janda, P. A. Gago, J. P. Peralta, L. M. Ferrer, L. A. Pugnaroni, E. Clément, D. Maza, I. Pagonabarraga, and A. Garcimartín, Clogging transition of many-particle systems flowing through bottlenecks, *Sci. Rep.* **4**, 7324 (2015).
- [66] E. Dressaire and A. Sauret, Clogging of microfluidic systems, *Soft Matter* **13**, 37 (2017).
- [67] H. Hinrichsen, Non-equilibrium critical phenomena and phase transitions into absorbing states, *Adv. Phys.* **49**, 815 (2000).
- [68] L. Corte, P. M. Chaikin, J. P. Gollub, and D. J. Pine, Random organization in periodically driven systems, *Nat. Phys.* **4**, 420 (2008).
- [69] S. Leitmann and T. Franosch, Nonlinear Response in the Driven Lattice Lorentz Gas, *Phys. Rev. Lett.* **111**, 190603 (2013).
- [70] P. Baerts, U. Basu, C. Maes, and S. Safaverdi, Frenetic origin of negative differential response, *Phys. Rev. E* **88**, 052109 (2013).
- [71] O. Bénichou, P. Illien, G. Oshanin, A. Sarracino, and R. Voituriez, Microscopic Theory for Negative Differential Mobility in Crowded Environments, *Phys. Rev. Lett.* **113**, 268002 (2014).
- [72] C. Reichhardt and C. J. O. Reichhardt, Negative differential mobility and trapping in active matter systems, *J. Phys.: Condens. Matter* **30**, 015404 (2018).
- [73] D. S. Fisher, Collective transport in random media: from superconductors to earthquakes, *Phys. Rep.* **301**, 113 (1998).
- [74] C. Reichhardt and C. J. O. Reichhardt, Depinning and nonequilibrium dynamic phases of particle assemblies driven over random and ordered substrates: a review, *Rep. Prog. Phys.* **80**, 026501 (2017).
- [75] C. Reichhardt and C. J. Olson, Colloidal Dynamics on Disordered Substrates, *Phys. Rev. Lett.* **89**, 078301 (2002).
- [76] Y. Fily, E. Olive, N. Di Scala, and J. C. Soret, Critical behavior of plastic depinning of vortex lattices in two dimensions: Molecular dynamics simulations, *Phys. Rev. B* **82**, 134519 (2010).
- [77] M. J. Higgins and S. Bhattacharya, Varieties of dynamics in a disordered flux-line lattice, *Physica C* **257**, 232 (1996).
- [78] C. Reichhardt and C. J. Olson Reichhardt, Charge Transport Transitions and Scaling in Disordered Arrays of Metallic Dots, *Phys. Rev. Lett.* **90**, 046802 (2003).
- [79] N. Di Scala, E. Olive, Y. Lansac, Y. Fily, and J. C. Soret, The elastic depinning transition of vortex lattices in two dimensions, *New J. Phys.* **14**, 123027 (2012).

- [80] C. Reichhardt and C. J. O. Reichhardt, Dynamic regimes and spontaneous symmetry breaking for driven colloids on triangular substrates, *Europhys. Lett.* **68**, 303 (2004).
- [81] C. Reichhardt and C. J. O. Reichhardt, Moving vortex phases, dynamical symmetry breaking, and jamming for vortices in honeycomb pinning arrays, *Phys. Rev. B* **78**, 224511 (2008).
- [82] X. Cao, E. Panizon, A. Vanossi, N. Manini, E. Tosatti, and C. Bechinger, Pervasive orientational and directional locking at geometrically heterogeneous sliding interfaces, *Phys. Rev. E* **103**, 012606 (2021).
- [83] M. B. Weissman,  $\frac{1}{f}$  noise and other slow, nonexponential kinetics in condensed matter, *Rev. Mod. Phys.* **60**, 537 (1988).
- [84] A. C. Marley, M. J. Higgins, and S. Bhattacharya, Flux Flow Noise and Dynamical Transitions in a Flux Line Lattice, *Phys. Rev. Lett.* **74**, 3029 (1995).
- [85] J. Jaroszyński, D. Popović, and T. M. Klapwijk, Universal Behavior of the Resistance Noise Across the Metal-Insulator Transition in Silicon Inversion Layers, *Phys. Rev. Lett.* **89**, 276401 (2002).
- [86] C. Reichhardt and C. J. O. Reichhardt, Noise at the Crossover from Wigner Liquid to Wigner Glass, *Phys. Rev. Lett.* **93**, 176405 (2004).